Adaptive waveform design for interference mitigation in SAR

Adaptive Waveform Design for Interference Mitigation in SAR

Claire Tierney[1], Bernard Mulgrew[2]

Abstract

This work details an interference mitigation scheme for synthetic aperture radar (SAR) which adapts the transmitted waveform spectrum to restore the quality of the scene range-profile based on the estimated interference spectrum. By expressing the estimation of the range-profile in the presence of correlated noise as a system identification problem, a cost function for the optimal waveform is derived. In order to respond effectively to changes in the radio frequency (RF) environment, adaptive waveform systems should perform waveform design on a small timescale, ideally on a pulse-to-pulse basis. Motivated by the need for a computationally efficient waveform design scheme, an alternative estimator is derived, which yields a closed form solution, which is shown to perform similarly to the optimal case. A series of test SAR images demonstrate the efficacy of this technique and are compared to the standard linearly frequency modulated signal and stretch processing outcome.

1. Introduction

Synthetic aperture radar(SAR) relies on large sections of uninterrupted bandwidth to obtain high resolution images. The dependence SAR systems have on wideband signals means they are particularly vulnerable to radio frequency interference (RFI) from neighboring spectral emissions which are often present in the increasingly crowded RFI spectrum. RFI causes degradation of the signal-to-interference plus noise ratio (SINR) which can mask and reduce the quality of the desired scene information. Furthermore, this effect raises the range profile (impulse response) sidelobes and causes significant degradation of the final SAR image quality as scene reflectors can become blurred, bright lines and other image aberrations may be seen across the image. As such, interference mitigation is a long standing area of interest for SAR and its solutions are varied

*This work was supported by the UK Engineering and Physical Sciences Research Council (EPSRC) [Grant No. EP/M507398/1] and Leonardo MW through the CASE Studentship scheme.

[1]C. Tierney (claire.tierney02@leonardocompany.com) is now with Leonardo MW.

[2]B. Mulgrew (b.mulgrew@ed.ac.uk) is with the School of Engineering, Institute for Digital Communications, The University of Edinburgh, UK.

in their effectiveness and computational complexity. The major body of work to address RFI in SAR is based around the use of linearly notched filters (see these works and references therein [1, 2]). While the notching removes the frequency bins that contain interference this also removes the useful signal information in these bins.

Therefore, these methods are only partially effective unless used alongside a sidelobe reduction algorithm as in [3] for additional computational cost. As an alternative to filtering, more recent SAR interference mitigation attempts now focus on estimating and separating RFI from the desired signal. These algorithms are generally sub-categorised into either parametric or non-parametric approaches. Parametric approaches model the RFI as sinusoidal waves but must do accurately in order to avoid introducing estimation bias [1, 4, 5]. Non-parametric methods exploit the statistical differences between the scene impulse response and the RFI, then subspace separation or filtering is applied in the frequency or time domains [6, 7, 8, 9]. These approaches are often highly computationally expensive or impose assumptions that may not always be true, for example in [6], the assumption is that the RFI eigenvalue bases are separable. Both parametric methods and non-parametric methods are generally restricted to dealing with very narrow-band interference ($< 1\%$ of radar bandwidth). Wider band approaches are possible, but the computational cost increases the wider band the RFI signal is [9, 10]. With RF transmissions becoming increasingly wideband in general with the demand for technology with higher information capacities, the need for wideband interference mitigation solutions, or more frequency diverse SAR transmissions to cope with the increasingly congested RF environment is apparent. The common point in the SAR mitigation literature is that the methods are performed on receive, or off-line post data collection. That is, the system does not respond to the threat adaptively in order to mitigate impact of interference. In this paper, we propose to alter the transmission on-the-fly as a means of adaptive interference mitigation.

"Cognitive" or adaptive waveform radar systems [11] have become of recent interest due to advancements in transmitter technology making on-the-fly design of transmit waveforms feasible[12]. This provides the potential for waveforms to be specifically tailored to the surrounding RF environment and the requirements of the radar mode. For the waveform design to be useful, the environment for which the waveform is being tailored must not have changed significantly between processing time-frames. To reduce the risk of waveform design redundancy, transmission of the next waveform should occur promptly after the previous received signal. This real-time scenario creates a race to design and transmit the next waveform before further scene changes invalidate the efforts of the design. This time-frame is regarded to be the major design challenge for adaptive waveform design systems and highlights the need for computationally efficient algorithms[13].

Within the past 10 years, waveform design efforts have become increasingly spectrum-conscious; either from the perspective of spectral coexistence with surrounding transmitters or from a performance perspective to exploit optimal occupation of the RF spectrum to yield enhanced performance metrics. The

spectral waveform design literature generally demonstrates one the following: 1) addition of small modifications to the standard linear frequency modulated (LFM) waveform to place nulls in the spectrum to remove RFI or to maintain co-existence with surrounding RF users [14, 15, 16, 17], 2) waveform design with forbidden bands where the spectrum cannot place energy or where it is optimal for avoiding transmitters [18, 19, 20, 21], 3) waveform optimization with forbidden regions while also attempting to optimize for another performance metric or feasibility constraint [22, 23, 24], 4) or more recently, by exploiting multiple-input-multiple output (MIMO)-radar to harness both frequency and spatial diversity to achieve spectral co-existence with other RF users [25, 26, 27, 28, 29].

Numerous recent waveform design methods consider the requirement for constant modulus amplitude to ensure maximum power efficiency at the receiver. Continually increasing phase-rate (frequency) is also desirable for implementation into electronically scanned radars, in other words, chirp-based waveforms either via a linear or non-linear frequency sweep. A time/frequency sweep permits the use of phase shifters to steer the transmitted beam - a necessary consideration for phased array radars. However many of the recent works for waveform design do not synthesize chirp-based waveforms and are also often based on iterative methods which may incur high computational complexity costs which radar hardware systems may struggle to implement on the-fly. These types of solutions are essential in understanding the required mathematics, but due to the computational complexity and iterative nature, these methods may be impractical on the fly, as convergence is unlikely be guaranteed within a transmit-receive window - this makes verification a challenge. This also does not satisfy the criteria for fast-response adaptivity.

Furthermore, the vast majority of the spectrum based waveform design techniques are based on optimizing for target detection. The common point across the spectral waveform design techniques is that they place gaps in the spectrum as it is optimal to do so for detection. However, a waveform optimal for detection is unlikely to be optimal for obtaining the best estimate of the range profile in SAR - creation of gaps in the spectrum is detrimental to the imaging performance. Although adaptive waveform design has been applied to a range of radar scenarios, to the authors knowledge, very little research has been done towards adaptive SAR systems for interference mitigation.

A SAR image is formed by obtaining the range profile of the desired scene from many successive angles - but the presence of RFI disrupts the quality of the range profile estimate. Each successive range-profile is altered due to the angle, and requires re-estimation. Given the ability to modify the spectral content of the waveform, it is then desirable to obtain the best possible estimate of the scene in the presence of interference. In this paper, this problem is set up as a least-squares system identification problem, by modifying the waveform such that it attempts to estimate the range profile which satisfies the minimum mean square error criterion.

With the aforementioned points considered, our motivations for this paper are summarised as follows: i) formulate a waveform design approach for SAR

to mitigate interference as a pre-emptive measure to maximise on-the-fly performance as an alternative to relying fully on post-processing interference, ii) provide a solution which is computationally efficient and viable for on-the-fly such that it is implementable with phase shifters (is chirp based), iii) perform interference mitigation which is able to tackle RFI that is greater than 1% of the bandwidth and does not increase in computational cost with increasing bandwidth iv) exploit use of frequency-domain system identification, which is not commonly used within radar applications.

This paper proposes a computationally efficient system-identification/waveform-design scheme for mitigating RFI in SAR on a pulse-to-pulse basis. No prior knowledge of the RFI is required. In doing so we also directly address the real-time challenge set out in [13].

The three main contributions of this paper are as follows:

1. *Joint range-profile/interference-spectrum estimation* We formulate the problem of SAR range-profile estimation in unknown interference as a frequency-domain system identification problem and through that formulation identify the optimal solution as the generalized least squares (GLS) estimator with a well-defined CRLB [30]. By extending concepts from frequency domain adaptive filtering [31] we develop an approximation to the GLS estimator that is based on the fast-Fourier transform (FFT). This technique also provides an estimate of the interference spectrum on-the-fly. It is also pertinent to note that the frequency-domain system identification estimation approach is free from inter-range-cell interference (IRCI) as pointed out in our preliminary results [32] and additionally in related work applied in an LFM-MIMO case [33]. A comparison of the proposed system identification scheme with OFDM is presented in [32].
2. *Adaptive waveform design* We develop a similar frequency domain approximation to the CRLB. We optimize this approximate CRLB with respect to the spectrum of the transmitted signal given the usual energy constraint on the waveform. This leads to a simple closed form solution that we prove is the global minimum for the approximate CRLB (given the energy constraint). These outcomes expand on preliminary results based on a heuristic approach to the waveform design which were presented in [34].
3. *Computationally efficient combined estimation/design/synthesis* To illustrate the potential of the above we combine them with a waveform-synthesis technique for nonlinear linear frequency modulation (NLFM) based on the stationary phase approximation (SPA) [35]. We consider this synthesis methodology because: i) its computational complexity is similar to what we propose above; (ii) NLFM meets the constant amplitude waveform constraint required for many practical systems and only requires phase shifters rather than time delays in electronically steered systems. We note however that the techniques mentioned above are not restricted to this form of synthesis or to NLFM. We show that the combined system has complexity of $\mathcal{O}(M \log_2(M))$ per transmitted pulse, where M

is the sum of range extent and transmit signal length in samples.

The paper is organized as follows: Section 2 describes an overview of the SAR system, sets up the problem in the time-domain, provides the system model and arrives at an optimization problem. In Section 3 the system identification problem is developed in the frequency domain via factorization with the FFT and the proposed time-constrained frequency domain solution. In Section 4 a frequency domain waveform optimization problem is proposed and Ssection 5 gives a possible method for waveform synthesis using non-linear signals. The performance of the proposed method is analyzed in Section 6, and SAR example simulated scenarios are demonstrated in Section 7 and finally concluding remarks are given in Section 8.

1.1. Notation

This paper adopts the following notation: **boldface** for vectors and matrices; the transpose, hermitian, diagonal and trace operators are denoted as $(.)^T$, $(.)^H$, diag(.) and tr(.) respectively. Linear convolution operator is $*$. The statistical expectation is denoted $E(.)$ and the covariance is cov(.).

2. SAR System Identification

2.1. SAR System Model

The SAR "stop-and-go" assumption is employed here such that a subsequent pulse is not transmitted until the return from the furthest scene range point is received. The nature of the SAR imaging scheme requires that each successive returned range profile is different from the previous returned pulse due to motion of the radar platform, and requires re-estimation on each waveform transmit-receive cycle. The full SAR data collection is over a burst of P coherent pulses. The pth transmitted signal is an N-dimensional, finite energy, finite duration and deterministic vector, where N is proportional to the pulse length τ_c and sampling rate $N = \tau_c f_s$.The system to be identified is a finite impulse response sequence $\mathbf{h}$ with K elements. Each element of the finite impulse response corresponds to one range cell in the SAR scene. The slant range resolution of one range cell is defined as $\delta_r = \frac{c}{2B}$ and $K = \frac{R_w}{\delta_r}$ where B is bandwidth in Hz, c is speed of light in ms^{-1}, R_w is scene extent length in meters. In this initial argument it is assumed that $N > K$, there are more transmitted signal samples than scene samples, such that the pulse duration τ_c is longer than the corresponding ground patch-propagation time length t_k - the time difference between the first sample in the SAR scene t_i and the last t_f, shown in Figure 1. This is an assumption typically used in spotlight SAR in combination with stretch processing [36]. For stripmap mode the pulse length is often chosen to be shorter than $\tau_c < t_k$ ($N < K$), a case that is explored in section IV. This system also assumes use of wideband sampling at the receiver, so the full bandwidth is stored on receive and stretch processing techniques are not applied. The pulse length τ_c has an upper limit such that the last returned

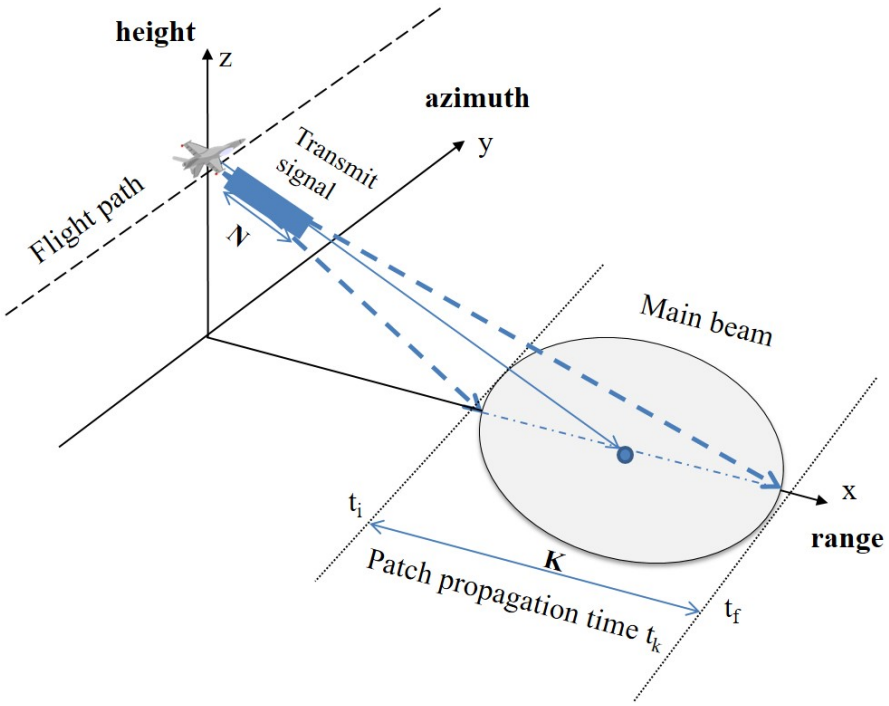

Figure 1: Spotlight SAR scene scenario with relative times in scene.

signal (from the furthermost range cell) has reached the radar before the next pulse is transmitted to avoid range-foldover effects, a common assumption in SAR [36].

The system block diagram shown in Figure 2 operates as per Algorithm 1 where p is the current pulse number in a coherent burst of P consecutive pulses. Steps 2 to 6 of the Algorithm describe the operations in the main blocks of Figure 2, starting in the top left hand corner and moving clockwise round the diagram. An LFM signal is used to start the process as it is nearly spectrally flat and aids the initial system identification calculation to estimate the interference spectrum by placing energy across the entire band. To allow full use of the synthetic aperture, all pulses are used to form the image. In this paper, back-projection [37] is used for image formation. The impulse response estimates at step 8 of Algorithm 1 are a convenient input for that technique. Other SAR imaging techniques, such as the more common polar format algorithm [37], require the associated frequency responses. As will be seen in Section 3, the latter are also provided by the System Identification block.

2.2. Time Domain Problem Formulation

Estimation of the range profile can be expressed as a discrete time problem. A returned range sample consists of a summation of all reflectivity points for the

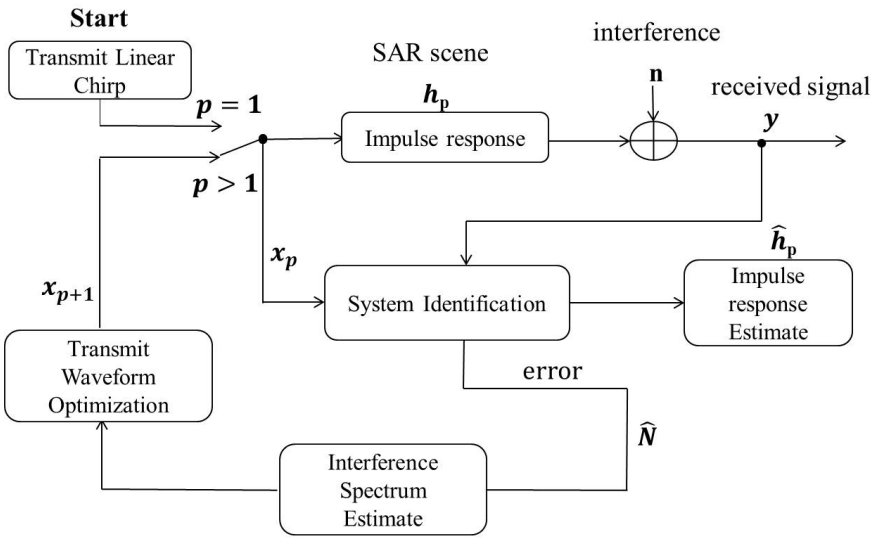

Figure 2: Pulse-to-pulse system flow chart.

Algorithm 1 Adaptive Waveform Design Scheme

Initialize: first pulse $\mathbf{x}_1$ is LFM

1: **for** $p = 1 : P$ **do**
2: Transmit pulse $\mathbf{x}_p$.
3: System identification: the transmitted pulse and the associated received signal $\mathbf{y}$ are used to estimate the impulse response $\mathbf{h}_p$ of the SAR scene and interference $\hat{\mathbf{N}}$ at the pth position of the radar.
4: Interference spectrum estimate; formed from the interference estimate.
5: Transmit waveform optimization: optimize transmit spectrum using estimate of interference spectrum.
6: Stationary phase waveform design: transmit spectrum is used to synthesize the next NLFM transmit pulse $\mathbf{x}_{p+1}$.
7: **end for**
8: Pass the collection of P impulse response estimates $\{\hat{\mathbf{h}}_p\}_{p=1}^{P}$ to the SAR image formation algorithm.

corresponding time sample. The fast-time observations at the receiver can be expressed as the convolution of the transmission sequence and the finite impulse response vector $\mathbf{h}_p$ as

$$y_p(k) = h_p(k) * x_p(k) + n_p(k) \tag{1}$$

where the transmitted waveform is $\mathbf{x}_p = \begin{bmatrix} x_p(0) & x_p(1) & \cdots & x_p(k) & \cdots & x_p(N-1) \end{bmatrix}^T$, p is transmitted pulse number and k is the kth sample of transmitted waveform where $k = (0, 1, \cdots, N-1)$. The finite impulse response is $\mathbf{h_p} = \begin{bmatrix} h_p(0) & h_p(1) & ... & h_P(K-1) \end{bmatrix}^T$.

The noise plus interference $\mathbf{n}$ is an $[N+K-1]$ dimensional vector with co-variance matrix $\mathbf{R}_{nn} = E[\mathbf{n}\mathbf{n}^H]$ and the interference is assumed to exist within the same bandwidth as the transmitted signal. To simplify the notation, we have dropped the subscript from the remainder of this Section. The linear convolution can also be expressed in matrix form as follows

$$\mathbf{y} = \mathbf{X}\mathbf{h} + \mathbf{n} \tag{2}$$

where $\mathbf{X}$ is a $(N+K-1) \times K$ rectangular and Toeplitz matrix where columns contain time shifted versions of the transmitted signal $\mathbf{x}_p$ and the received signal is of corresponding length $(N+K-1)$. The terms after the data vector can be zero as they correspond to before or after the transmitted signal.

$$\mathbf{X} = \begin{bmatrix} x(0) & 0 & ... & 0 \\ x(1) & x(0) & ... & 0 \\ \vdots & & & \\ & \vdots & \ddots & \\ x(K-1) & x(K-2) & ... & x(0) \\ x(K) & x(K-1) & ... & x(1) \\ \vdots & & & \\ x(N-1) & x(N-2) & \dots & x(N-K) \\ 0 & x(N-1) & \dots & x(N-K+1) \\ \vdots & & & \\ 0 & 0 & \dots & x(N-1) \end{bmatrix}$$

Because we assume that the impulse response is finite and we collect all the returns from the transmitted signal, equation (2) defines $N+K-1$ equations in K unknowns and is thus an overdetermined system. The case where this assumption is not justified is considered in [32]. The impulse response of the scene can be estimated as [38]

$$\hat{\mathbf{h}} = (\mathbf{X}^H \mathbf{R}_{nn}^{-1} \mathbf{X})^{-1} \mathbf{X}^H \mathbf{R}_{nn}^{-1} \mathbf{y} \tag{3}$$

Using the estimator for the generalized least squares (GLS) problem directly is computationally expensive and initially the interference covariance is unknown.

If the noise and interference source is white, the covariance matrix is reduced to a diagonal of the variances $\mathbf{R}_{nn} = \sigma_n^2 \mathbf{I}$ giving the simpler ordinary least squares (OLS) estimator.

$$\hat{\mathbf{h}} = (\mathbf{X}^H \mathbf{X})^{-1} \mathbf{X}^H \mathbf{y} \tag{4}$$

Generalized least squares is equivalent to applying ordinary least squares to a whitened version of the system [38]. In [34] we motivated the waveform design for least-squares by postulating that if the spectra for the transmit signal is matched to the interference, that the ordinary least squares solution can be used. Here we seek a more formal solution. Waveform design is employed to achieve the optimal estimation of the scene impulse response in the presence of correlated interference according to the least-squares solution. Waveform design for the optimal least squares solution should try to minimize the error to find the best fit for $\hat{\mathbf{h}}$. The Cramer-Rao lower bound (CRLB) for the generalized least squares estimate of the impulse response vector is given by the spread of the covariances[38]

$$\mathrm{cov}(\mathbf{h} - \hat{\mathbf{h}}) = E[(\mathbf{h} - \hat{\mathbf{h}})(\mathbf{h} - \hat{\mathbf{h}})^H] = (\mathbf{X}^H \mathbf{R}_{nn}^{-1} \mathbf{X})^{-1} \tag{5}$$

Therefore waveform design for SAR system identification in the presence of interference can be formulated as the following constrained optimization problem

$$\begin{aligned} \min_{\mathbf{x}} \quad & \mathrm{tr}(\mathbf{X}^H \mathbf{R}_{nn}^{-1} \mathbf{X})^{-1} \\ \text{s.t.} \quad & \mathbf{x}^H \mathbf{x} = E_T \end{aligned} \tag{6}$$

where E_T is the energy in the transmitted signal. The authors are unaware of an existing analytical method to solve this expression. A possible numerical optimization procedure is particle swarm optimization (PSO), a global optimization technique [39]. This can be applied to the optimization problem to find the best overall waveform under the constraint of energy. As it is an iterative method PSO potentially requires a large number of computations to find the solution - especially as matrix inversion is required on each iteration. We propose a more computationally efficient approach to estimating the impulse response by factorizing with the DFT and expressing the problem in the frequency domain. The following steps aim to approximate the CRLB of (6) to facilitate a tractable analytic solution that is computationally efficient. However we use (6) and its solution through PSO, as a benchmark to quantify the performance loss incurred by the approximation.

3. System Identification and Interference Estimation

3.1. Cyclic Extension

By describing the problem in the frequency domain we can exploit factorization with the discrete Fourier transform (DFT) to create a computationally efficient least squares expression. Matrices that are square, circulant and Toeplitz factor conveniently with the discrete Fourier transform.

From here onwards define $M = N + K - 1$, where M, as mentioned in the introduction, is dependent on the sum of range extent and transmit signal length. Equation (2) can be re-written as

$$\mathbf{y} = \begin{bmatrix} \mathbf{X} & [*] \end{bmatrix} \begin{bmatrix} \mathbf{h} \\ \mathbf{0}_{N-1} \end{bmatrix} + \mathbf{n}$$

(recalling that $\mathbf{X}$ is an $(M \times K)$ matrix) where $[*]$ in an $(M \times (N-1))$ matrix of "don't care" terms and $\mathbf{0}_{N-1}$ is a column vector of $N-1$ zeros. The above will hold for any value of $[*]$. The ith column of $\mathbf{X}$, for the column set $\{\forall i : 1 < i \leq K\}$, is obtained by applying $i-1$ downward cyclic shifts to the first column at $i = 1$, defined as $\mathbf{x}_{c1}$. If this downward cyclic shift process is extended to all the columns in the set $\{\forall i : 1 < i \leq M\}$, it assigns columns to $[*]$ and defines the $(M \times M)$ circulant Toeplitz matrix, $\mathbf{X}_c$. Thus equation (2) can be written as

$$\mathbf{y} = \mathbf{X}_c \begin{bmatrix} \mathbf{h} \\ \mathbf{0}_{N-1} \end{bmatrix} + \mathbf{n} \tag{7}$$

The circulant Toeplitz matrix admits the factorisation [40]

$$\mathbf{X}_c = \mathbf{F}^H \mathrm{diag}\left\{\mathbf{F}\mathbf{x}_{c_1}\right\} \mathbf{F} \tag{8}$$

where $\mathbf{F}$ is an $(M \times M)$ DFT matrix such that $\mathbf{F}^H\mathbf{F} = \mathbf{I}_M$ and $\mathbf{I}_M$ is an $(M \times M)$ identity matrix. It should be noted that this cyclic extension is an artifact of the signal processing in the receiver and is not applied to the signal at transmission.

3.2. Frequency Domain Solution

Proceeding, we seek an alternative non-optimal estimator in place of the computationally expensive, exact estimator in (4) . Applying Fourier transforms to both sides of time-domain circulant matrix equation (7) and using the identity property, where $\mathbf{F}$ is an M-point discrete Fourier transform, gives

$$\mathbf{F}\mathbf{y} = \mathbf{F}\mathbf{X}_c\mathbf{F}^H\mathbf{F} \begin{bmatrix} \mathbf{h} \\ \mathbf{0}_{N-1} \end{bmatrix} + \mathbf{F}\mathbf{n} \tag{9}$$

Now the expression for circulant-Toeplitz matrices given in (8) can replace $\mathbf{X}_c$ and again using the identity property gives

$$\mathbf{Y} = \mathbf{\Omega}\mathbf{H} + \mathbf{N} \tag{10}$$

where $\mathbf{\Omega} = \mathbf{F}\mathbf{X}_c\mathbf{F}^H = \mathrm{diag}\left\{\mathbf{F}\mathbf{x}_1\right\}$, $\mathbf{Y} = \mathbf{F}\mathbf{y}, \mathbf{H} = \mathbf{F} \begin{bmatrix} \mathbf{h} \\ \mathbf{0}_{N-1} \end{bmatrix}$ and $\mathbf{N} = \mathbf{F}\mathbf{n}$. Given an expression of the system model in the frequency domain, a corresponding generalized least squares estimate for $\mathbf{H}$

$$\hat{\mathbf{H}} = (\mathbf{\Omega}^H\mathbf{D}^{-1}\mathbf{\Omega})^{-1}\mathbf{\Omega}^H\mathbf{D}^{-1}\mathbf{Y} \tag{11}$$

where

$$E[\mathbf{N}\mathbf{N}^H] = \mathbf{F}\mathbf{R}_{nn}\mathbf{F}^H = \mathbf{D} \tag{12}$$

Equation (11) is an approximation since it does not embody the constraint on the estimate inherent in (7), specifically

$$\mathbf{0}_{N-1} = [\ \mathbf{0}_{N-1,K} \quad \mathbf{I}_{N-1}\ ]\mathbf{F}^{-1}\hat{\mathbf{H}} \tag{13}$$

where $\mathbf{0}_{N-1}$ is an column vector of $N-1$ zeros, $\mathbf{0}_{N-1,K}$ is an $(N-1)\times(K)$ matrix of zeros and $\mathbf{I}_{N-1}$ is an $(N-1)\times(N-1)$ identity matrix.

The noise-covariance matrix $\mathbf{R_{nn}}$ is positive definite as there will always be some level of background white noise due to thermal noise. The eigen-decomposition can be written as

$$\mathbf{R_{nn}} = \mathbf{V}\mathbf{\Lambda}\mathbf{V}^H$$

where Λ is a diagonal matrix of the eigenvalues and $\mathbf{V}$ is the orthonormal matrix such that $\mathbf{V}^H\mathbf{V} = \mathbf{I}$ whose columns are the corresponding eigenvectors. The eigenvectors also define the Karhunen-Loeve transform(KLT) of the noise vector $\mathbf{V}^H\mathbf{n}$ .The elements of $\mathbf{V}^H\mathbf{n}$ are orthogonal and therefore uncorrelated since

$$E[\mathbf{V}^H\mathbf{n}\mathbf{n}^H\mathbf{V}] = \mathbf{V}^H\mathbf{R}_{nn}\mathbf{V} = \mathbf{V}^H\mathbf{V}\mathbf{\Lambda}\mathbf{V}^H\mathbf{V} = \mathbf{\Lambda}$$

The KLT has history of being approximated by signal-independent transforms such as the DFT and the discrete cosine transforms due to its complexity. This approximation of the DFT to the KLT has lead to the DFT being used to approximately orthogonalize signals. The justification for this was initially used in Markov-1 processes [41]. Examples can be found in the fields of frequency-domain adaptive filtering [31, 42] and in radar, where the frequency snapshot model uses the orthogonalization assumption [43] and also in [20] to justify use of the frequency domain to avoid a matrix inversion.

Assuming that now, due to the application of the DFT, the frequency domain samples are uncorrelated, the off-diagonal elements of the frequency domain interference covariance matrix $\mathbf{D}$ will be approximately zero and are disregarded allowing a vector expression $\tilde{\mathbf{D}}$ to be formed from the diagonal replacing $\mathbf{D}$ in (11).

$$\tilde{\mathbf{D}} = \mathrm{diag}(\mathbf{D})$$

This provides a simple estimate in the frequency domain which is element wise. With this approximation we have what might be called a "doubly-diagonal" system, both the input signal matrix Ω and the noise covariance matrix $\tilde{D}$ are diagonal. The GLS of (11) reduces to OLS with the added benefit that we do not require knowledge to $\tilde{D}$ to form the estimate.

$$\hat{H}_i = \frac{Y_i}{\Omega_i} \qquad i = (1, 2, \cdots, M) \tag{14}$$

This frequency domain least squares problem has the same number of knowns and unknowns, which was not the case in the time-domain problem of (2) which

had fewer unknowns. Similar to methods used in frequency domain adaptive filtering [31, 42] an approximation to the LS estimate of (3) is obtained by projecting the estimate provided by (14) onto the feasible set of solutions defined by the constraint of (13).

$$\hat{\mathbf{h}}_c = [\ \mathbf{I}_K \quad \mathbf{0}^T_{N-1,K}\ ]\mathbf{F}^{-1}\hat{\mathbf{H}} \tag{15}$$

where $\mathbf{I}_K$ is an $K \times K$ identity matrix. This operation removes the additional $N-1$ samples that was added to the original time domain problem to allow the problem to be expressed in the frequency domain via representation via circular convolution. The removal of the extra $N-1$ terms in the time domain also acts as noise-removal. This works best when $N > K$, as noise removal performance is proportional to the number of samples N removed. This effect on performance is demonstrated in section VI.C. Here we are also exploiting the assumption that the impulse response is finite. In actuality, energy from the antenna extends beyond the mainbeam into the sidelobes, but generally only the returns corresponding from the range-swath are desired. This range swath is assumed to be finite. This has been studied in other systems whereby an infinite impulse response is represented as finite, and the incurred error on estimate is generally shown to be small [44].

We further note that the same assumption of a finite and known length of range swath is made in standard stretch processing for LFM-based SAR systems [36]. The corresponding estimate of the time-constrained frequency response is then:

$$\hat{\mathbf{H}}_c = \mathbf{F}(\begin{bmatrix} \hat{\mathbf{h}}_c \\ \mathbf{0}_{N-1} \end{bmatrix}) \tag{16}$$

which finally, provides an estimate $\hat{\mathbf{N}}$ of the interference $\mathbf{N}$ where:

$$\hat{N}_i = Y_i - \Omega_i \hat{H}_i \tag{17}$$

and from which an estimate of the interference spectrum $\tilde{\mathbf{D}}$ can be formed in a straightforward way, $\tilde{\mathbf{D}} = \mathbf{g}(|\hat{N}_i|^2)$, where $\mathbf{g}$ is a moving average filter which is applied to smooth the spectral estimate.The unfiltered spectral estimate $\mathbf{D} = |N_i|^2|$ may exhibit large sample to sample fluctuations as this estimate results from a single realization of the spectrum. Directly using this spectral estimate would also yield a waveform that is high in sample-to-sample fluctuation and may not provide a good representation of the true spectral distribution.

The TCFDE of (11),(15) and (16) provide an approximation to the GLS of (3) that is DFT based. This approach is more computationally efficient than the direct GLS estimator. Using the TCFDE is thus better suited to the relatively long impulse responses that are typical in SAR, as larger DFT dimensions scale better computationally than matrix inversions. In addition the TCFDE does not require explicit knowledge of the interference covariance matrix $\mathbf{R}_{nn}$ and provides a mechanism through (16) to estimate the spectrum of that interference "on-the-fly". The latter capability facilitates adaptive waveform design.

4. Waveform Optimization

We now have three possible estimators for the impulse/frequency response. Equation (3) provides the optimal solution if the interference covariance matrix is known. Its performance is given by (5). The unconstrained frequency domain estimate of (11) is the simplest computationally but it is liable to give poor performance as it has no capacity for noise reduction and it approximates linear convolution with circular convolution. The constrained frequency domain estimate of (14), (15) and (16) is an improvement on (14) because it enforces linear convolution and reduces noise through (15) and (16). The performance of this constrained frequency domain estimate are explored further in [32]. Central to many adaptive waveform design (AWD) methods is the judicious choice of a cost function. Ideally we would like to use a cost function that accurately reflects the performance of the radar, e.g. (6). However, if we chose to implement (3), the optimization of (6) is a still a major challenge. Often a cost function is chosen that is an approximation to or a bound on the actual performance metric because no convenient closed form solution for the metric exists. For example, in AWD for detection [45], the asymptotic performance is used as a cost function because no closed form solution for the detector performance on finite data sets exists. Similarly, in bearing estimation [46], the CRLB is used even through the estimator does not achieve that bound. Again no closed form expression for the performance of the estimator exists. Thus while we advocate the use of the constrained estimate of (14),(15) & (16) for estimating the impulse response, we use the unconstrained estimate of (11) to provide a simple cost function for the waveform design that leads to a closed form expression for the transmitted spectrum in terms of the spectrum of the interference. As argued earlier the performance of the unconstrained estimate is poorer than the constrained one and thus we are optimizing an upper bound on the performance of the constrained estimate.

Thus, we address the "doubly-diagonal" system discussed in Section 3, i.e. a system defined by (10) which is not constrained by (13) and where $\mathbf{D}$ is a positive definite diagonal matrix with ith diagonal element D_i. It follows that the GLS estimate is given by (11) and, by analogy to (3) and (5), the error covariance of that estimate is

$$\mathrm{cov}(\mathbf{H}-\hat{\mathbf{H}}) = E[(\mathbf{H}-\hat{\mathbf{H}})(\mathbf{H}-\hat{\mathbf{H}})] = (\mathbf{\Omega}^H\mathbf{D}^{-1}\mathbf{\Omega})^{-1} \tag{18}$$

The trace of this covariance matrix gives a single metric, P, that quantifies the performance of the estimate

$$P \triangleq \mathrm{tr}((\mathbf{\Omega}^H\mathbf{D}^{-1}\mathbf{\Omega})^{-1}) = \sum_{i=0}^{M-1}\frac{D_i}{|\Omega_i|^2} \tag{19}$$

As with (6), the quality of the estimate is limited by the total transmit energy E_T that is available for the signal. In discrete time, using Parseval's theorem, this is

$$E_T = \sum_{i=0}^{M} E_i = \sum_{i=0}^{M}|\Omega_i|^2 = \sum_{k=0}^{N-1}|x_i|^2 \tag{20}$$

For ease of notation we define the energy at each frequency sample as

$$E_i = |\Omega_i|^2 \tag{21}$$

We seek to minimize the performance metric P subject to the energy constraint of (20) and the property that energy is non-negative. Formally this optimization problem can be expressed as

$$\begin{aligned} \min_{\mathbf{E}} \quad & \sum_{i=0}^{M-1} \frac{D_i}{E_i} \\ \text{s.t.} \quad & \sum_{i=0}^{M-1} E_i = E_T \\ & E_i > 0, \ \forall i. \end{aligned} \tag{22}$$

where $\mathbf{E} = [\ E_0 \quad E_1 \quad ... \quad E_{M-1}\ ]^T$. The appeal of this optimization problem, unlike (6), is that it admits, as we now show, a simple closed-form solution.

The method of Lagrange provides the solution. However the presence of the inequality constraints usually requires the use of the Karush-Kuhn-Tucker (KKT) conditions (c.f. chapter 5 of [47]). However here the inequality constraints are straightforward. Our approach is to first solve the optimization problem without the inequality constraints using the Lagrangian dual function [47] and then identify all the possible solutions. We show that only one of these solutions satisfies the inequality constraints, We also show, using the methodology set out in [48], that the single solution that satisfies the inequality constraints is a minimum.

Without the inequality, (22) reduces to

$$\begin{aligned} \min_{\mathbf{E}} \quad & f(\mathbf{E}) \\ \text{s.t.} \quad & g(\mathbf{E}) - E_T = 0 \end{aligned} \tag{23}$$

where, we define $f(\mathbf{E}) = \sum_i \frac{D_i}{E_i}$ and $g(\mathbf{E}) = \sum_i E_i$. The Lagrange function is

$$L(\mathbf{E}, \lambda) = f(\mathbf{E}) + \lambda(g(\mathbf{E}) - E_T) \tag{24}$$

and λ is the Lagrange multiplier. Necessary conditions for a solution are obtained by setting the gradient of $L(\mathbf{E}, \lambda)$ to zero. Thus

$$\nabla f(\mathbf{E}) + \lambda \nabla g(\mathbf{E}) = \mathbf{0}_M \tag{25}$$

where $\nabla f(\mathbf{E})$ indicates the gradient of $f(\mathbf{E})$ and $\mathbf{0}_M$ is a vector of M zeros. Hence

$$\frac{\partial L}{\partial E_i} = -\frac{D_i}{E_i^2} + \lambda = 0, \quad \forall i \tag{26}$$

and thus

$$\lambda = \frac{D_i}{E_i^2}, \quad \forall i. \tag{27}$$

Since $\mathbf{D}$ is a diagonal and positive definite, $D_i > 0$ and hence $\lambda > 0$. It follows that

$$E_i = \frac{\pm\sqrt{D_i}}{\sqrt{\lambda}}. \tag{28}$$

To solve for λ we apply the energy constraint (20) to give

$$E_i = E_T \frac{\pm\sqrt{D_i}}{\sum_i \pm\sqrt{D_i}}. \tag{29}$$

This equation defines 2^M possible solutions to (23). The solutions are are dependent on the choice of sign on the square root of each D_i. Consistently choosing either all positive or all negative roots, gives

$$E_i = E_T \frac{\sqrt{D_i}}{\sum_i \sqrt{D_i}}. \tag{30}$$

This particular solution satisfies the non-negative energy constraint of (22). The remaining solutions all contain combinations of both positive and negative values for the squares roots of each D_i. Hence, irrespective of the sign of the denominator $\sum_i \pm\sqrt{D_i}$, these solutions all contain both positive and negative values for each of the energy terms E_i and hence they do not satisfy the non-negative energy constraint. Only (30) satisfies the necessary conditions for a solution to (22).

For brevity we will call (30) frequency domain waveform optimization (FDWO). While the development here is similar to [20], the result is distinctly different. In [20] a detection problem is addressed whereas here we address system identification problem. Thus it is not surprising that the results might be different and it is interesting to note that there is no sense of "water-filling" (c.f.[20]) here or conclusion that signal energy should be directed to areas of the spectrum where the interference density is relatively low. Rather (30) suggests a more competitive approach. An example signal outcome $\mathbf{E}$ for a given interference energy $\mathbf{D}$ is shown in Figure 3.

5. Waveform Synthesis

The previous section has determined the energy distribution across the frequency band. The following describes a possible method of synthesizing a time domain signal according to the spectrum described in (30). We desire a frequency modulated (FM) signal with constant amplitude modulus and spectrum distribution. The stationary phase approximation (SPA), a standard technique used for synthesis of nonlinear FM waveforms [35, 49], provides synthesis according to these criteria. The synthesis technique detailed here is independent from the TCFDE scheme. If desired, this would allow alternative waveform synthesis techniques to be used in conjunction with the TCFDE scheme, provided that they synthesize a signal with the desired frequency spectrum e.g. using

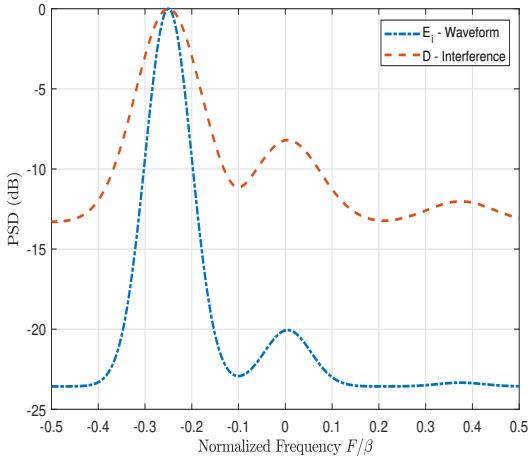

Figure 3: Illustrative example demonstrating signal energy outcome from (30) is proportional to the interference energy.

OFDM techniques or non-chirp based methods. The particular merit of the SPA method is that it is non-iterative and will provide a solution provided that the instantaneous frequency is continually increasing - either at a linear rate (LFM) or non-linearly (NLFM). SPA relies on the assumption that amplitude variations are very slow compared to phase variations, which results in most of the energy becoming concentrated around stationary points. Applying a Fourier Transform to a general chirp signal with amplitude and phase variation creates an intractable integral. A large majority of the contribution to the Fourier spectrum occurs where the change of oscillation of the function is at its lowest, a stationary point, this can be exploited to calculate an approximation to the integral. This occurs when the frequency is monotonically increasing and the amplitude variations are much slower than the phase variations. This gives rise to the following relationship between the time and frequency domains [35, 49]

$$\ddot{\psi}(t) = \frac{C}{\mathbf{E}(f)} \tag{31}$$

The relationship between t and f is given by:

$$\dot{\psi}(t) = 2\pi f \tag{32}$$

where $\dot{\psi}(t)$ is the phase change over time and $\ddot{\psi}(t)$ is the change in frequency over time. These expressions allow synthesis of a NLFM waveform according to a desired spectrum $E(f)$ by continually increasing the phase (instantaneous frequency). As demonstrated in Figure 4 the output spectrum is an approximation to the input spectrum as provided by $E(f)$. While this method is not exact, it is a computationally simple approach for waveform synthesis compared

to more precise but computationally complex methods demonstrated in the literature [50]. Furthermore, a precise replication of the input spectrum may not be required as $E(f)$ is calculated based on an estimate of the interference $D(f)$ provided by the system identification on the prior pulse. By approximating to the spectrum of the interference, small errors in the interference estimate are not further propagated into the performance of the system identification of the current pulse.

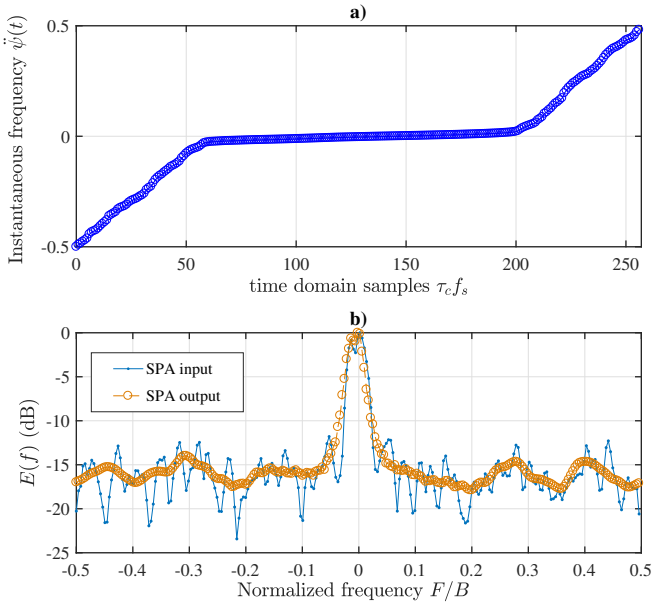

Figure 4: a): Input spectrum given by $\mathbf{E}(f)$ (blue) and resultant transmit spectrum given by SPA. b): Synthesized transmit signal. Non-linear upward sweep in instantaneous frequency gives non-linear "chirp" waveform.

6. Performance Evaluation

6.1. Simulation Experiment Set-Up

The following section demonstrates the performance of the TCFDE technique combined with the waveform optimization and design method in terms of the error in the impulse response estimate. Additionally this section aims to evaluate the associated loss in performance that is introduced in the development of the alternative frequency domain estimate, the TCFDE, which approximates the direct estimator (5). The assumed knowledge to perform the simulations is as follows; the transmitted signal and its spectral representation, the received signal and the length of the range-swath, which corresponds to the impulse response length K. The known frequency domain representations

of the received and transmitted signal, $\mathbf{Y}$ and $\mathbf{\Omega}$ are processed according to steps (14)-(16), to provide an estimate of the impulse response $\hat{\mathbf{h}}$. The norm of the simulated impulse response vector $\mathbf{h}$ is normalised to unity such that $\sum_{k=0}^{K-1} |h_p(k)|^2 = 1$. Narrowband interference is generated by constructing uncorrelated complex normal samples of length M then passed through a bandpass filter to create correlated interference samples so that the interference lies within 10% of the overall signal bandwidth. The impulse response estimate $\hat{\mathbf{h}}$ is evaluated and 1000 trials are executed at each configuration. The energy in each transmit signal and the total nominal bandwidth is constant across generated waveforms.

To quantify the performance of the following waveform design and estimator pairs under test, and as is usual with the assessment of system identification algorithms, we calculate the norm of the error vector (trace of the error covariance matrix) between the actual complex impulse response value $\mathbf{h}$ and the estimated value $\hat{\mathbf{h}}$.

$$\rho \triangleq \mathrm{tr}(\mathrm{cov}(\mathbf{h} - \hat{\mathbf{h}})) = E[(\mathbf{h} - \hat{\mathbf{h}})^H (\mathbf{h} - \hat{\mathbf{h}})] \tag{33}$$

This metric is calculated for the ensemble of pseudo-randomly generated scene impulse responses and interferences as described above. The interference estimate ρ_n is calculated in the same manner as (33), replacing $\hat{\mathbf{h}}$ for $\hat{\mathbf{N}}$. TCFDE is a discrete time technique which can be used for any corresponding transmit signal bandwidth, time and sampling frequency - the important metric for performance being the relationship between K the number of samples corresponding to the scene length and N the transmitted signal length. For the following section B, the relationship is shown for a ratio of $K/N = 0.25$. This is incrementally altered in section C by increasing the scene length and keeping transmit signal length constant.

6.2. Performance Relative to Interference Power

As the radar system is limited by an upper bound of energy, there will exist a critical interference level where the placement of energy into the same band as the interferer will no longer provide a useful estimate of the impulse response as high sidelobes and noise override the signal. To demonstrate the performances relative to interferer strength, the following simulations increase the interference power to lower the overall signal to interference and noise ratio (SINR) i.e. - increased interference strength while keeping the waveform signal constant, lowers the SINR value at each consecutive simulation experiment.

$$\mathrm{SINR} = \frac{\sum_{m=0}^{M} |\Omega_m|^2}{\sum_{m=0}^{M} E[|D_m|^2]} \tag{34}$$

where the power of the interferer is a finite value. The total power in the interference is increased at each simulation to demonstrate the result on performance with increasing interference as demonstrated in Figure 5. The dependency on the interference spectrum relative to the transmitted signal is demonstrated

in (30). As this necessitates that performance for the FDWO-NLFM-TCDFE method is limited by the level of interference power, the performance with increasing RFI strength is demonstrated here via simulation. Simulated examples demonstrate how performance error varies with interference power for the following waveform and impulse response estimation techniques;

1. LFM with stretch processing
2. Initial LFM- TCFDE
3. FDWO-NLFM-TCFDE
4. GLS optimized with PSO with known interference covariance $\mathbf{R}_{nn}$

Where 1) is the standard SAR configuration, 2) is the first step of the system identification process as shown in Figure 2, 3) is the waveform designed after the initial LFM transmit-receive loop using the suboptimal estimator and 4) is the global optimal solution constrained under energy, but without amplitude or phase constraints. For a comparison to TCFDE, the PSO method is used to solve the original optimization problem given in (6). The PSO optimization is only under the constraint of energy and finds the optimal time-domain waveform solution $\mathbf{x}_{pso}(t)$ based on the interference co-variance matrix $\mathbf{R}_{nn}$. The PSO waveform is generated by using the estimated NLFM waveform for the initial conditions and numerically searching for the optimal waveform to minimize the error in the impulse response estimate (6).

6.2.1. LFM-TCFDE

In the adaptive system shown in Figure 2 the first transmitted pulse is used to obtain an estimate of the interference frequency profile $\hat{\mathbf{N}}$ and a scene estimate $\hat{\mathbf{h}}_1$. If there is no correlated noise present, the flat spectrum is optimal for the impulse response estimation. In correlated noise this first LFM pulse is expected to perform sub-optimally as it is not yet shaped according to the interference as this is initially assumed to be unknown. This method simultaneously obtains interference and scene data on the same pulse, which if successful, is an advantage compared to passive approaches that do not collect scene data while collecting interference data. This first LFM pulse then allows an estimate of $\hat{\mathbf{D}}$ and subsequently enables the design of the next NLFM pulse to obtain an enhanced estimate by shaping the spectrum of the waveform according to (30). While this approach to initializing the system is not the optimal solution, it provides performance as least as good as LFM-stretch (Figure 5) until much higher interference regions. If the interference spectrum is already known, this step can be omitted and the FDWO-NLFM-TCFDE process can be used.

6.2.2. FDWO-NLFM-TCFDE

Leading from the initial interference spectral estimate given by the LFM-TCFDE the performance of the FDWO-NLFM-TCDFE is indicative of the best system performance. Note that its performance is also dependent on the quality of the interference estimate from the prior pulse. In this way, it serves as an indicator of the overall system performance. It is shown in Figure 5 that using

this scheme consistently improves performance compared with transmitting the LFM signal- both compared to evaluation via stretch processing and TCFDE.

6.2.3. CRLB

The CRLB is a waveform-dependent measure of the best possible performance attainable by a specific designed waveform in an interference characterized by covariance matrix $\mathbf{R}_{nn}$ as shown in (5). The true known simulated R_{nn} is used along with the time-domain SPA synthesized waveform to provide the CRLB value. Therefore, it is a useful tool to evaluate any performance losses in the adaptive system. These losses account for both: i) the estimation of the interference to design the waveform and ii) those incurred via the TCFDE impulse response approximation to the direct GLS estimate approach in (5). These include the diagonalization assumption used to form the expression in (14) and the approximation of linear-to circular convolution and re-constraining this value in the time domain in (15) back to linear convolution. The CRLB has been calculated for both the LFM waveform and the NLFM waveform used in the FDWO-NLFM-TCDFE combination and are labeled CRLB-LFM and CRLB-NLFM respectively in Figure 5. The larger performance gap between in LFM-TCFDE and CRLB-LFM compared to FDWO-NLFM-TCFDE and CRLB-NLFM can be attributed to the larger error in interference estimate, shown in Figure 6.

6.2.4. PSO-GLS

This result serves as an indicator of an absolute lower bound of performance for a given interference. Using the simulated interference covariance matrix, the PSO algorithm searches for the global optimal time-domain waveform solution constrained only by energy (6). In the absence of structure constraints in the form of phase or amplitude, while this waveform offers the best performance, this is both computationally expensive and not amenable to physical implementation. Furthermore, note that this method is not considered here as a viable method for waveform synthesis as the convergence time cannot be guaranteed, and therefore does not meet the adaptivity constraints. Using this optimal technique provides a means to demonstrate the performance losses incurred in the FDWO-NLFM-TCFDE method through; (i) using the alternative frequency-domain estimator TCFDE (ii) using SPA to constrain the time-domain waveform to be constant amplitude and increasing in phase over time.

Further, if the CRLB-NLFM estimate (given the FDWO-NLFM-TCFDE) is compared to the PSO-GLS, the difference shows the performance lost by forcing the amplitude and phase structure via the SPA. For moderate levels of interference there is minimal performance impact of constraining the waveform. The difference between the FDWO-NLFM-TDFDE and PSO show the costs of using an alternative estimator and SPA waveform synthesis.

6.2.5. Interference Estimate

The performance error of the interference spectrum estimate $\hat{\mathbf{D}}$ is shown for comparison between the initial (LFM) ($p = 1$) and adapted FDWO-NLFM-TCFDE pulse ($p = 2$) and finally a subsequent third pulse ($p = 3$) using the

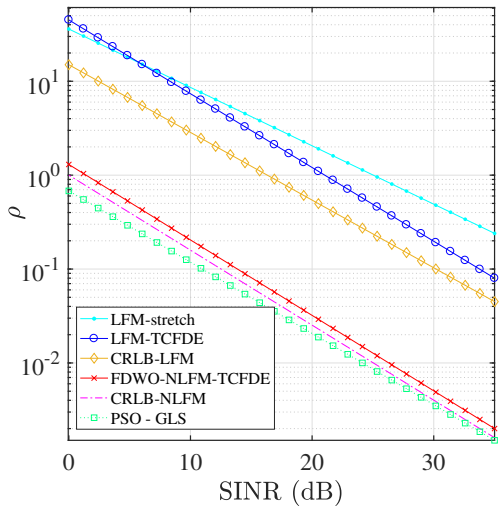

Figure 5: Performance error norm results from 35dB to 0dB at $K/N = 0.25$ on a semi-log plot

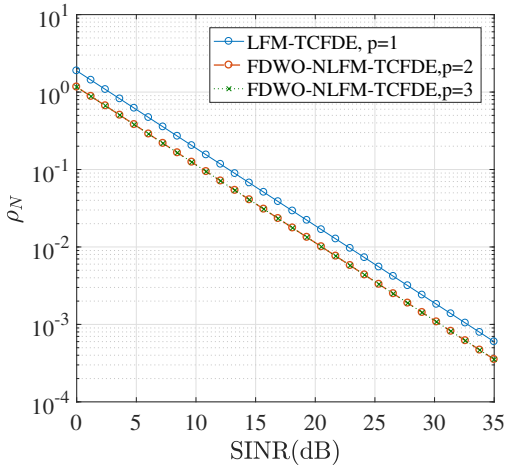

Figure 6: Mean squared error for interference spectrum estimate for initial pulse $p = 1$, adapted pulse $p = 2$, and the subsequent pulse $p = 3$

interference estimate from the prior pulse in Figure 6. There is minimal performance gap between ($p = 2$) and subsequent estimation demonstrating that for static interference further pulses are not required to improve the interference estimate.

6.3. Performance for Relative Scene Size

Shown in (15), the TCFDE method constrains the frequency-response estimate in the time-domain to re-express the estimate without assuming circular convolution. This step removes $N-1$ samples to provide the original $K-1$ range cells, which as a by-product removes noise that was present in the additional $N-1$ samples.

The ability to remove noise/error originating from the estimation process is therefore dependent on the ratio between the discrete representation of the scene impulse response $K-1$ and the transmitted pulse length $N-1$.

When $N > K$ (for small scene sizes) the removal is comparatively large but when $K > N$, there is less error removal. The following simulated experiment demonstrates different scene lengths relative to the same pulse length and its effect on the TCFDE performance. The longer the pulse-length relative to the scene size, the larger the performance gain. The performance error improves linearly with the removal of samples. This effect is shown in Figure 6.3 for increasing scene sizes while keeping the pulse length N constant. This is demonstrated for interference levels of 5dB, 10dB and 15dB SINR. The higher the interference level, the higher the gradient at which the performance drops off due to additional noise suppression. While the method is operational for larger scene sizes it is at reduced performance as additional noise suppression is greater for smaller scenes.

6.4. Computational Complexity of FDWO-NLFM-TCDFE

An overview of the scaling of the processing required for one pulse is presented in this section. The larger the input scene length K and pulse length N, the higher the number of operations required for the signal processing for the TCDFE scheme per pulse. This method initially appears to be low-computational complexity as this is a non-iterative process. The computational complexity of the full adaptive cycle can be broken down into the following three stages.

6.4.1. System identification and interference estimation

The system identification process complexity is given by the number of operations between calculating $\hat{\mathbf{h}}$ and $\hat{\mathbf{N}}$. The upper limit on the computational complexity can be given by considering the computations required each iteration for; element-wise division in (14) which increases linearly with the vector size M so there are M divisions, the DFT and inverse DFT in (17) $\mathcal{O}(M \log_2 M)$ [51] and finally the element-wise multiplication used in calculating $\hat{\mathbf{N}}$. Calculating $\hat{\mathbf{h}}$ and $\hat{\mathbf{N}}$ requires M-point DFTs as given in (14) and (15)

$$\mathcal{C}_1 = \mathcal{O}(M) + \mathcal{O}(M \log_2 M)$$

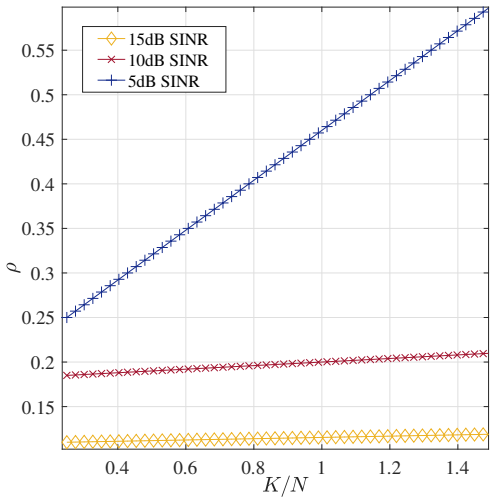

Figure 7: Performance impact for increasing impulse response lengths at varying levels of SINR

6.4.2. Waveform optimization and design

The waveform design can be carried out via the expression in (30). This requires calculation of the total energy E_T which is a summation over M points and scales linearly. Calculating $E_i(F)$ then requires $\mathcal{O}(M)$ for division of M.

$$\mathcal{C}_2 = \mathcal{O}(M)$$

6.4.3. Waveform Synthesis

The implementation of SPA requires a cumulative summation of the estimated optimized waveform spectrum $\mathbf{E}_i(F)$ in order to use relationship between change in frequency and time as shown in (32). This uses the addition and multiplication operator. Linear interpolation is also required for obtaining frequency values for the set of time samples corresponding to $\ddot{\psi}(t)$. Linear interpolation computational complexity depends both on the number of existing data points M and the number of data points to be interpolated. For this case, the number of points to be interpolated is the same as the original number of data points. The largest operation performed by an interpolation algorithm is sorting the each data point into the relevant interval between two existing points given as $(2M)\log_2(2M)$. After this, the linear interpolation is simple and performs two additions and one multiplication so scales linearly.

$$\mathcal{C}_3 = \mathcal{O}(M) + \mathcal{O}(M\log_2(M))$$

Overall the FDWO-NLFM-TCDFE based adaptive cycle computational complexity scales with $\mathcal{O}(M\log_2 M)$ as the dominant complexity term per waveform design-transmission/azimuth point.

6.5. Performance Discussion

Compared with alternative SAR mitigation techniques discussed in the introduction, this approach has the following advantages: i) there is no introduction of sidelobes as a result of interference mitigation attempts - as observed in filtering techniques. Gaps are not produced in the spectrum which is another source of sidelobes in spectrum filtering methods, ii) the RFI spectrum is a by-product of the frequency domain system identification, therefore no iterative processing or best-fit estimates for an RFI model are required, potentially at the expense of introducing estimation bias as in parametric methods iii) there is no inherent assumption that the RFI and signal must have different statistical properties as seen in non-parameteric methods iv) computational complexity does not scale with number of interfereres or bandwidth. Compute time is irrespective of bandwidth and the performance is dependent on overall SINR.

The performance is however limited at higher interference levels as shown in Figure 5, for lower SINR the MSE increases. To maintain performance, the solution will eventually have to admit gaps into the spectrum, at which point a trade off between loss of resolution and interference mitigation must be considered, this case is explored in the following publication [52]. This dependence on SINR also implies that, although, for larger bandwidths the system does not incur additional computational cost, there is an adverse effect in performance as this causes an overall increase in SINR, and therefore MSE.

7. SAR Scenario Example

We consider a spotlight SAR system and assume an approximately circular antenna pattern. The carrier frequency is f_c=3GHz, transmitted signal bandwidth is B_w=500MHz, and the number of time domain samples N =600. The number of range bins $K = (T_f - T_i) \times f_s = 200$. The estimated impulse response vectors collected at each azimuth point is then processed using the back-projection image formation algorithm. The test scene image is shown in Figure 8. which represents the back-projection image created from the actual impulse responses of the scene without added interference. The test SAR scene represents a static aircraft on the ground and is used to exemplify the effects of interference on the final SAR image.

7.1. Constant Interference Source

In this example the interference source does not change its spectral content $\mathbf{N}$ across the SAR data collection for all azimuth points. After a two-pulse cycle, the waveform does not need to adapt further and continues to transmit the designed pulse $\mathbf{x}_2$. The initial pulse identifies an approximate estimate of the interference spectrum $\mathbf{N}_1$ and the adapted waveform provides an improved estimate of the interference $\mathbf{N}_2$ as demonstrated previously. We compare the SAR images created from the LFM-stretch method and the FDWO-NLFM-TCFDE approach. Figure 9.a shows the LFM-stretch processing image at 10dB

SINR. In Figure 9b, the image represents the result from the FDWO-NLFM-TCFDE method at 10dB SINR. Comparing these images show that the FDWO-NLFM-TCDFE method has provided a sharper more focused image than the stretch method. Increasing to 1dB SINR causes the image quality to degrade significantly as it reaches the upper limit of its estimation capability, but still yields a more focused outcome than LFM-Stretch at the same SINR.

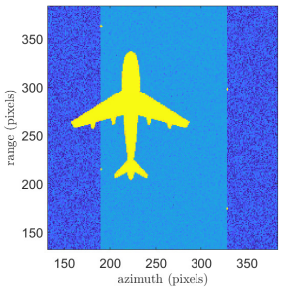

Figure 8: Test SAR image representing a stationary ground-based aircraft on top of a road with grass either side, created using back-projection with no interference

7.2. Dynamic Interference Source

In the following example the interference spectrum is changing pulse-to-pulse by an upwards sweep in frequency across the bandwidth frequency which the radar signal is using and the total width of the narrowband interference is kept constant. The total SINR is kept constant at 5dB. This scenario demonstrates a need to employ waveform design regularly enough to compensate for interference changing pulse-to-pulse. Figure 10b shows for comparison the LFM-Stretch result at 5dB SINR. The image heavily degrades if the pulse is not adapted at all after the initial interference estimate is obtained. There is slight reduction in image quality qualitatively comparing the image obtained from adapting every 100 pulses and the image waveform adapted on every pulse. Using fewer adaptive cycles may be desirable in cases where overall computational load needs to be reduced.

8. Conclusion

This work has presented a combined system identification and waveform design scheme for mitigating RF interference in SAR on a pulse-to-pulse basis. It has been demonstrated that under the TCFDE scheme, to minimize the error in the scene impulse response, the waveform spectral content is proportional to the energy of the RF interference according to the relationship in (30). Using cyclic extension as an artifact in the processing allowed formulation of a constrained frequency domain estimate and a low complexity method for calculating the scene impulse response was derived. Results have demonstrated that this scheme

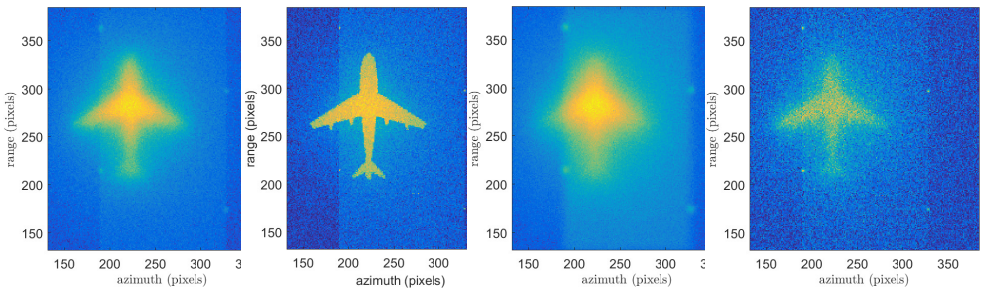

Figure 9: Simulated SAR images formed with back projection with RFI PSD unchanged across collection aperture. The following waveform-estimation approaches and SINR levels are tested: a) LFM-Stretch at 10dB SINR b) FDWO-NLFM-TCFDE at 10dB SINR c)LFM-Stretch at 1dB SINR d) FDWO-NLFM-TCFDE at 1dB

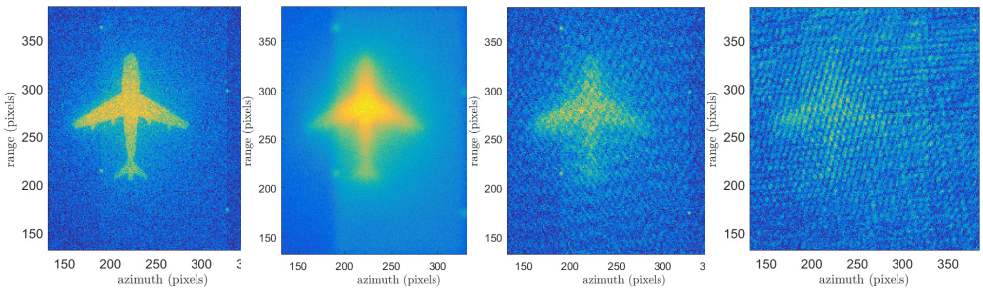

Figure 10: Simulated SAR images formed with back projection with RFI present at 5dB SINR and updated RFI PSD at varying rates with specified waveform-estimation approaches as follows: a) FDWO-NLFM-TCFDE Adapted every pulse at 5dB SINR b) LFM Stretch at 5dB SINR c)FDWO-NLFM-TCFDE adapted every 100 pulses d) FDWO-NLFM-TCFDE adapted to first pulse only

can be used for cases where the transmitted signal length is either greater than or less than the ground patch propagation time, but at the expense of loss of performance due to less noise-removal. This scheme is most suitable for the scenarios where the bandwidth availability is compromised from leakage from neighboring transmitters or other unwanted in-band interference returning usage of the entire spectrum to the radar. Compared to spectrum friendly approaches where areas of the spectrum are avoided due to interference, this scheme competes and aims to return usage of the entire spectrum.

References

[1] T. Miller, L. Potter, J. McCorkle, RFI suppression for ultra wideband radar, IEEE Transactions on Aerospace and Electronic Systems 33 (4) (1997) 1142–1156.

[2] X. Luo, L. M. H. Ulander, J. Askne, G. Smith, P. O. Frolind, RFI suppression in ultra-wideband SAR systems using LMS filters in frequency domain, Electronics Letters 37 (4) (2001) 241–243.

[3] J. K. Abend, Radio and tv interference extraction for ultrawideband radar, Proc.SPIE 2487 (1995) 2487 – 2487 – 11.

[4] L. H. Nguyen, T. Ton, D. Wong, M. Soumekh, Adaptive coherent suppression of multiple wide-bandwidth RFI sources in SAR, Proc. SPIE 5427 (2004) 1–16. doi:10.1117/12.542466.
URL http://dx.doi.org/10.1117/12.542466

[5] J. O.Ojowu Jr, RFI suppression for synchronous impulse reconstruction UWB radar using RELAX, Int. J. Remote. Sens. Appl. 3 (March 2013) 33–46.

[6] F. Zhou, M. Tao, Research on methods for narrow-band interference suppression in synthetic aperture radar data, IEEE Journal of Selected Topics in Applied Earth Observations and Remote Sensing 8 (7) (2015) 3476–3485. doi:10.1109/JSTARS.2015.2431916.

[7] F. Zhou, M. Tao, Z. Bao, Suppression of narrow-band interference in SAR data, in: 2014 IEEE Geoscience and Remote Sensing Symposium, 2014, pp. 227–230. doi:10.1109/IGARSS.2014.6946398.

[8] M. Tao, F. Zhou, J. Liu, Y. Liu, Z. Zhang, Z. Bao, Narrow-band interference mitigation for SAR using independent subspace analysis, IEEE Transactions on Geoscience and Remote Sensing 52 (9) (2014) 5289–5301. doi:10.1109/TGRS.2013.2287900.

[9] M. Tao, F. Zhou, Z. Zhang, Wideband interference mitigation in high-resolution airborne synthetic aperture radar data, IEEE Transactions on Geoscience and Remote Sensing 54 (1) (2016) 74–87. doi:10.1109/TGRS.2015.2450754.

[10] H. Liu, D. Li, Y. Zhou, T. K. Truong, Joint wideband interference suppression and SAR signal recovery based on sparse representations, IEEE Geoscience and Remote Sensing Letters 14 (9) (2017) 1542–1546. doi:10.1109/LGRS.2017.2721425.

[11] S. Haykin, Cognitive radar: A way of the future, Signal Processing Magazine, IEEE 23 (1) (2006) 30–40.

[12] R. Calderbank, S. Howard, B. Moran, Waveform diversity in radar signal processing, Signal Processing Magazine, IEEE 26 (1) (2009) 32–41.

[13] D. Cochran, S. Suvorova, S. Howard, B. Moran, Waveform libraries, Signal Processing Magazine, IEEE 26 (1) (2009) 12–21.

[14] I. W. Selesnick, S. U. Pillai, R. Zheng, An iterative algorithm for the construction of notched chirp signals, in: 2010 IEEE Radar Conference, 2010, pp. 200–203.

[15] I. W. Selesnick, S. U. Pillai, Chirp-like transmit waveforms with multiple frequency-notches, in: 2011 IEEE RadarCon (RADAR), 2011, pp. 1106–1110.

[16] M. Picciolo, J. D. Griesbach, K. Gerlach, Adaptive LFM waveform diversity, in: 2008 IEEE Radar Conference, 2008, pp. 1–6.

[17] K. Gerlach, M. Frey, M. Steiner, A. Shackelford, Spectral nulling on transmit via nonlinear FM radar waveforms, Aerospace and Electronic Systems, IEEE Transactions on 47 (2) (2011) 1507–1515.

[18] W. Rowe, P. Stoica, J. Li, Spectrally constrained waveform design [sp tips & tricks], Signal Processing Magazine, IEEE 31 (3) (2014) 157–162.

[19] A. Aubry, A. De Maio, M. Piezzo, A. Farina, Radar waveform design in a spectrally crowded environment via nonconvex quadratic optimization, Aerospace and Electronic Systems, IEEE Transactions on 50 (2) (2014) 1138–1152.

[20] S. Kay, Optimal signal design for detection of Gaussian point targets in stationary Gaussian clutter/reverberation, Selected Topics in Signal Processing, IEEE Journal of 1 (2007) 31–41.

[21] H. He, P. Stoica, J. Li, Waveform design with stopband and correlation constraints for cognitive radar, in: 2010 2nd International Workshop on Cognitive Information Processing, 2010, pp. 344–349.

[22] A. Aubry, V. Carotenuto, A. D. Maio, Forcing multiple spectral compatibility constraints in radar waveforms, IEEE Signal Processing Letters 23 (4) (2016) 483–487.

[23] Y. Huang, M. Piezzo, V. Carotenuto, A. De Maio, Radar waveform design under similarity, bandwidth priority, and spectral coexistence constraints, in: 2017 IEEE Radar Conference (RadarConf), 2017, pp. 1142–1147.

[24] A. Aubry, A. De Maio, L. Martino, M. A. Govoni, Phase-only radar waveform design for spectrally dense environments, in: 2019 IEEE Radar Conference (RadarConf), 2019, pp. 1–6.

[25] Z. Cheng, B. Liao, Z. He, Y. Li, J. Li, Spectrally compatible waveform design for mimo radar in the presence of multiple targets, IEEE Transactions on Signal Processing 66 (13) (2018) 3543–3555.

[26] Z. Cheng, C. Han, B. Liao, Z. He, J. Li, Communication-aware waveform design for mimo radar with good transmit beampattern, IEEE Transactions on Signal Processing 66 (21) (2018) 5549–5562.

[27] B. Tang, J. Li, Spectrally constrained mimo radar waveform design based on mutual information, IEEE Transactions on Signal Processing 67 (3) (2019) 821–834.

[28] S. Shi, Z. Wang, Z. He, Z. Cheng, Spectrally compatible waveform design for mimo radar with isl and papr constraints, IEEE Sensors Journal 20 (5) (2020) 2368–2377.

[29] X. Wang, G. Zhang, Y. Zhang, Q. Wang, H. Leung, Design of spectrally compatible waveform with constant modulus for colocated multiple-input multiple-output radar, IET Radar, Sonar Navigation 13 (8) (2019) 1373–1388.

[30] T. Amemiya, Advanced Econometrics, Havard University Press, 1985.

[31] J. J. Shynk, Frequency-domain and multirate adaptive filtering, Signal Processing Magazine, IEEE 9 (1992) 14 – 37.

[32] C. Tierney, B. Mulgrew, Waveform independent range profile reconstruction for SAR, in: International Conference on Radar Systems (Radar 2017), 2017, pp. 1–6.

[33] M. AlShaya, M. Yaghoobi, B. Mulgrew, Frequency domain system identification for high resolution irci-free collocated mimo radar, in: 2018 15th European Radar Conference (EuRAD), 2018, pp. 134–137.

[34] C. Tierney, B. Mulgrew, Adaptive waveform design with least-squares system identification for interference mitigation in SAR, in: 2017 IEEE Radar Conference (RadarConf), 2017, pp. 0180–0185.

[35] M. Richards, Fundamentals of Radar Signal Processing, Second Edition, McGraw-Hill Education, 2014.

[36] C. V. J. Jakowatz, D. E. Wahl, P. H. Eichel, D. C. Ghiglia, P. A. Thompson, Spotlight-Mode Synthetic Aperture Radar: A Signal Processing Approach, Springer US, 1996.

[37] M. Soumekh, Synthetic Aperture Radar Signal Processing with MATLAB Algorithms, New York: J. Wiley, May 1999.

[38] G. Goodwin, G. Goodwin, R. Payne, Dynamic System Identification: Experiment Design and Data Analysis, Developmental Psychology Series, Academic Press, 1977.

[39] J. Kennedy, R. Eberhart, Particle swarm optimization, in: Neural Networks, 1995. Proceedings., IEEE International Conference on, Vol. 4, 1995, pp. 1942–1948 vol.4.

[40] R. M. Gray, Toeplitz and circulant matrices: A review, Commun. Inf. Theory 2 (3) (2005) 155–239.

[41] M. Hamidi, J. Pearl, Comparison of the cosine and Fourier transforms of Markov-1 signals, IEEE Transactions on Acoustics, Speech, and Signal Processing 24 (5) (1976) 428–429.

[42] S. Haykin, Adaptive Filter Theory (3rd Ed.), Prentice-Hall, Inc., Upper Saddle River, NJ, USA, 1996.

[43] H. L. Van Trees, Optimum Array Processing, John Wiley & Sons, Inc., New York, USA, 2002.

[44] H. Wold, P. Faxer, On the specification error in regression analysis, Ann. Math. Statist. 28 (1) (1957) 265–267.

[45] S. Sen, OFDM radar space-time adaptive processing by exploiting spatio-temporal sparsity, Signal Processing, IEEE Transactions on 61 (1) (2013) 118–130.

[46] W. Huleihel, J. Tabrikian, R. Shavit, Optimal adaptive waveform design for cognitive MIMO radar, Signal Processing, IEEE Transactions on 61 (20) (2013) 5075–5089.

[47] S. Boyd, L. Vandenberghe, Convex Optimization, Cambridge University Press, New York, NY, USA, 2004.

[48] M. A. H. Nerenberg, The second derivative test for constrained extremum problems, International Journal of Mathematical Education in Science and Technology 22 (2) (1991) 303–308.

[49] E. Fowle, The design of FM pulse compression signals, IEEE Transactions on Information Theory 10 (1) (1964) 61–67.

[50] L. K. Patton, B. D. Rigling, Phase retrieval for radar waveform optimization, Aerospace and Electronic Systems, IEEE Transactions on 48 (4) (2012) 3287–3302.

[51] T. H. Cormen, C. E. Leiserson, R. L. Rivest, C. Stein, Introduction to Algorithms, Third Edition, 3rd Edition, The MIT Press, 2009.

[52] C. Tierney, B. Mulgrew, Interference mitigation in sar via gapped spectrum waveform design, in: 2019 International Radar Conference (RADAR), 2019, pp. 1–6.

***Credit Author Statement**

Claire Tierney: Conceptualization, Methodology, Software, Validation, Writing – original draft preparation**,** Formal analysis, Investigation, Visualization **Bernard Mulgrew**: Conceptualization, Methodology, Supervision, Writing - Review & Editing, Project administration, Funding acquisition